3-13-2007

Electric field-induced phase transitions in (111)-, (110)-, and (100)-oriented Pb(Mg1/3Nb2/3)O3 single crystals

X. Zhao
Iowa State University

W. Qu
Iowa State University

Xiaoli Tan
Iowa State University, xtan@iastate.edu

A. A. Bokov
Simon Fraser University

Z.-G. Ye
Simon Fraser University

Electric field-induced phase transitions in (111)-, (110)-, and (100)-oriented $Pb(Mg_{1/3}Nb_{2/3})O_3$ single crystals

X. Zhao, W. Qu, and X. Tan*
Department of Materials Science and Engineering, Iowa State University, Ames, Iowa 50011, USA

A. A. Bokov and Z.-G. Ye
Department of Chemistry, Simon Fraser University, Burnaby, B.C. Canada V5A 1S6

(Received 22 June 2006; revised manuscript received 15 January 2007; published 13 March 2007)

Electric field-induced phase transitions were investigated in (111), (110), and (100) thin platelets of relaxor ferroelectric $Pb(Mg_{1/3}Nb_{2/3})O_3$ single crystals with electric fields applied along the ⟨111⟩, ⟨110⟩, and ⟨100⟩ directions, respectively. Temperature dependences of complex dielectric permittivity, pyroelectric current and dielectric hysteresis loops were investigated. Electric field-temperature (*E*-*T*) phase diagrams were proposed for the different directions of the field. Alongside with the high-temperature ergodic relaxor phase and the low-temperature glassy nonergodic relaxor phase existing at $E=0$, the ferroelectric phase may appear in the diagram at the fields higher than the threshold field (E_{th}). The temperature of the first-order transition between ergodic relaxor and ferroelectric phases (T_C) was located in field cooling and field heating after field-cooling regimes. For the ⟨111⟩ field direction, T_C is higher and E_{th} is lower than for the other directions. For the ⟨100⟩ direction, T_C is the lowest and E_{th} is the highest. The critical point bounding the $T_C(E)$ line when the field is applied in ⟨111⟩ direction [Z. Kutnjak, J. Petzelt, and R. Blinc, Nature **441**, 956 (2006)] is not observed in the ⟨110⟩ and ⟨100⟩ directions up to the highest applied field of 7.5 kV/cm. Extrapolation of experimental data suggests that the critical point for the ⟨110⟩ and ⟨100⟩ directions (if any) can be expected only at much higher fields. In the hysteresis loops experiments performed after zero-field cooling, the lower temperature limit is determined above which a ferroelectric phase can be induced from the frozen glassy state at a given field strength or the polarization of the induced ferroelectric phase can be reversed. This limit is located at much lower temperatures in the (100) platelet than in the (110) or (111) platelets. An additional ferroelectric rhombohedral to ferroelectric orthorhombic phase transition occurs in the (110) platelet at high electric fields (~20 kV/cm). The mechanisms of the field-induced transformation from the glassy nonergodic relaxor phase or the ergodic relaxor phase to the ferroelectric phase are discussed.

DOI: 10.1103/PhysRevB.75.104106 PACS number(s): 77.80.Bh, 77.22.Ch, 77.84.Dy

I. INTRODUCTION

Complex perovskite $Pb(Mg_{1/3}Nb_{2/3})O_3$ (PMN), a prototype relaxor ferroelectric compound, exhibits both a strong frequency dispersion and a high relative permittivity with a broad dielectric peak around $T_m=265$ K.[1,2] The origin of the relaxor ferroelectric behavior can be traced back to the structure of the compound, where nanometer scale (<5 nm) 1:1 cation ordering exists on the *B* site of the ABO_3 perovskite.[3–7] Superimposed on the nanoscale chemical ordering is the nanoscale polar ordering in PMN crystals.[8] The polar nanoregions nucleate at the Burns temperature $T_B=650$ K. Upon cooling below about 300 K, the polar nanoregions begin to grow, reaching about 7 nm at 10 K, with the most significant growth taking place around the intrinsic Curie temperature $T_{C0}=213$ K.[9–15] The structure of the polar regions is slightly distorted along the ⟨111⟩ direction, yet the long-range structure preserves cubic symmetry without any phase transition down to liquid He temperature.[9–15] Recent first-principles-based simulations showed that in the temperature range from T_B to 300 K, the polar nanoregions are essentially the same as the cation ordered domains.[16,17]

The most fascinating aspect of PMN lies in its nonergodic states under bias electric fields.[18–29] The polar nanoregions in PMN can grow into micrometer-sized ferroelectric domains when driven by external electric fields, which corresponds to a field-induced phase transition.[20,30,31] The transition kinetics study has shown that when a static field is applied to a zero-field-cooled crystal along the ⟨111⟩ direction, the phase transition takes place abruptly after an incubation period.[23–26] During incubation under 3 kV/cm at 175 K, the polar nanoregions coarsen up to ~70 nm; the percolation of the coarsened polar regions leads to the ferroelectric state with a rhombohedral symmetry.[26] The polarization in the induced ferroelectric state is reversible only within a temperature range, bounded by the upper limit of Curie temperature T_C and the lower limit of the temperature below which the ferroelectric spontaneous polarization is clamped. Both these limits are functions of bias field.[19–21] The intrinsic Curie temperature T_{C0} (determined by zero field heating after field cooling), 213 K, lies in between the clamping temperature and T_C. The lowest threshold bias field E_{th} to trigger the relaxor cubic to the ferroelectric rhomobohedral transition is found around the temperature T_{C0}. When the field is applied along the ⟨111⟩ direction, E_{th} was observed to be 1.75 kV/cm.[20]

The current understanding of the electric field-induced phase transition in $Pb(Mg_{1/3}Nb_{2/3})O_3$ is built almost entirely on experimental observations of (111) thin crystals with the field along the ⟨111⟩ direction. Limited, though inconsistent reports on (110) and (100) crystals have clearly shown that they behave differently from (111) crystals under electric

fields. Schmidt *et al.*[29] observed that when the electric field was applied along the ⟨100⟩ direction, T_{C0} was 13 K lower than when the field was along the ⟨110⟩ and ⟨111⟩ directions. In addition, the hysteresis loop measurements indicated different remanent polarization P_r and coercive field E_c among the three directions. Arndt *et al.*[30] noticed that a ferroelectric rhombohedral phase could be induced at 180 K with a bias field of 10 kV/cm along ⟨111⟩ or ⟨110⟩, but not along ⟨100⟩.Westphal and colleagues[18] observed a number of optically detected Barkhausen jumps under a reversed field of 3.3 kV/cm along the ⟨110⟩ direction at 221 K. Ye and Schmid[20] observed the electric field-induced phase transition in all (111), (110), and (100) platelets. A monodomain state was realized in (111) platelets under a field as low as 2.2 kV/cm (in the ⟨111⟩ direction) around T_{C0}, but a multidomain state invariantly resulted in the (100) platelet even under 150 kV/cm (in the ⟨100⟩ direction). Recently, Lushnikov *et al.*[32] measured the phonon velocity in PMN crystals under a bias field of 5 kV/cm along the ⟨111⟩, ⟨110⟩, and ⟨100⟩ directions and speculated that different phases may have been triggered by electrical stimuli.

Compared with the phase transition induced by electric fields along the ⟨111⟩ direction, the transition under ⟨110⟩ or ⟨100⟩ fields is expected to be more complicated because the external field is not aligned with the local polarization axis of the polar nanoregions. As a result, the electric field (E) vs temperature (T) phase diagrams with fields applied along the ⟨110⟩ and the ⟨100⟩ directions in PMN crystals have yet to be established. The present work studied the orientation dependence of the electric field-induced phase transition in PMN single crystals and proposed the E-T phase diagrams for (110)- and (100)-oriented crystals poled along the ⟨110⟩ and ⟨100⟩ directions, respectively.

II. EXPERIMENTAL PROCEDURE

$Pb(Mg_{1/3}Nb_{2/3})O_3$ single crystals were grown via a high temperature solution process from the flux of $PbO\text{-}B_2O_3$.[33,34] Thin slices with broad faces parallel to the (111), (110), and (100) crystallographic planes were cut and polished. Gold electrodes measuring approximately 6 mm^2 were deposited by sputtering. The electric field was applied across the thickness, which was around 0.3 mm, of the thin slices.

Dielectric permittivity and loss as a function of temperature were measured under bias fields of 0, 3.0, 5.0, and 7.5 kV/cm with LCR meters (HP-4284A or Keithley 3330) in conjunction with a Delta 9023 environmental chamber. A heating-cooling rate of 2 K/minute was used during measurements. The bias field was switched on at room temperature, and immediately after that the crystal was cooled down to 123 K (field-cooling test) and heated up back to the room temperature (field-heating after field-cooling test). Between measurements with different bias fields, crystal samples were thermally annealed at 373 K to eliminate possible history effect. Thermal depolarization current was measured using a picoammeter (Keithley 484) at a heating rate of 2 K/min. The polarization hysteresis loops of the crystal platelets were displayed by a RT-66A ferroelectric test system (Radiant Technologies). For hysteresis loop measurements, the crystals were first cooled to 123 K without electric field at a cooling rate of 4 K/min. Then the temperature was set, in sequence, to 153, 173, 193, 213, and 233 K to let the chamber warm up. When the temperature was stabilized for 10 minutes at the setpoint, a hysteresis loop was measured at a peak-to-peak field of ±20 kV/cm.

III. EXPERIMENTAL RESULTS

A. Dielectric properties under zero bias

The dielectric permittivity of the (111), (110), and (100) single crystal platelets upon cooling without bias field is shown in Fig. 1. The characteristic broad peaks and strong frequency dispersion are clearly seen. The T_m at 1 kHz was found to be 268 K for all three orientations.

B. Thermal depolarization measurement

The Curie temperature under zero-field heating after field cooling (intrinsic Curie temperature), T_{C0}, was measured by monitoring the thermal depolarization current of 10 kV/cm field-cooled crystals. From the measurement, T_{C0} is found to be ~217 K for the (111) and (100) platelets, and ~213 K for the (110) platelet. The integration of the current with respect to time indicates the development of macroscopic polarization. Such an integration process leads to the polarization vs temperature curves shown in Fig. 2. The macroscopic polarization developed by 10 kV/cm field cooling from room temperature to 183 K was measured as 33, 28, and 21 $\mu C/cm^2$ for the (111), (110), and (100) platelets, respectively. The development of macroscopic polarization is a manifestation of the electric field-induced relaxor to normal ferroelectric phase transition. Furthermore, the polarization values support a rhombohedral structure with $\langle 111\rangle_{cubic}$ polar direction.[19] This can be seen from the fact that $33(\mu C/cm^2) \times \cos 35.3^\circ = 27(\mu C/cm^2) \approx 28(\mu C/cm^2)$; $33(\mu C/cm^2) \times \cos 54.7^\circ = 20(\mu C/cm^2) \approx 21(\mu C/cm^2)$, where 35.3° is the angle between the $\langle 110\rangle_{cubic}$ and $\langle 111\rangle_{cubic}$ directions, and 54.7° between the $\langle 100\rangle_{cubic}$ and $\langle 111\rangle_{cubic}$ directions.

C. Dielectric properties upon field cooling

The field-induced phase transition is further characterized by detailed dielectric measurements. The temperature dependence of dielectric permittivity and loss under field-cooling conditions for the (111), (110), and (100) crystals are shown in Fig. 3. With the electric field applied along the ⟨111⟩ direction, a sharp dielectric anomaly was detected at 222 K under E=3.0 kV/cm, indicating a first-order induced phase transition. With the field increased to 5.0 kV/cm, the dielectric anomaly occurred at a higher temperature, 238 K, and became broader. At a still higher field of 7.5 kV/cm, the dielectric anomaly immersed into the broad dielectric peak around T_m [Fig. 3(a)]. These results are consistent with previous studies that showed a correlation between increasing field strength and a smoother induced phase transition process.[20,22]

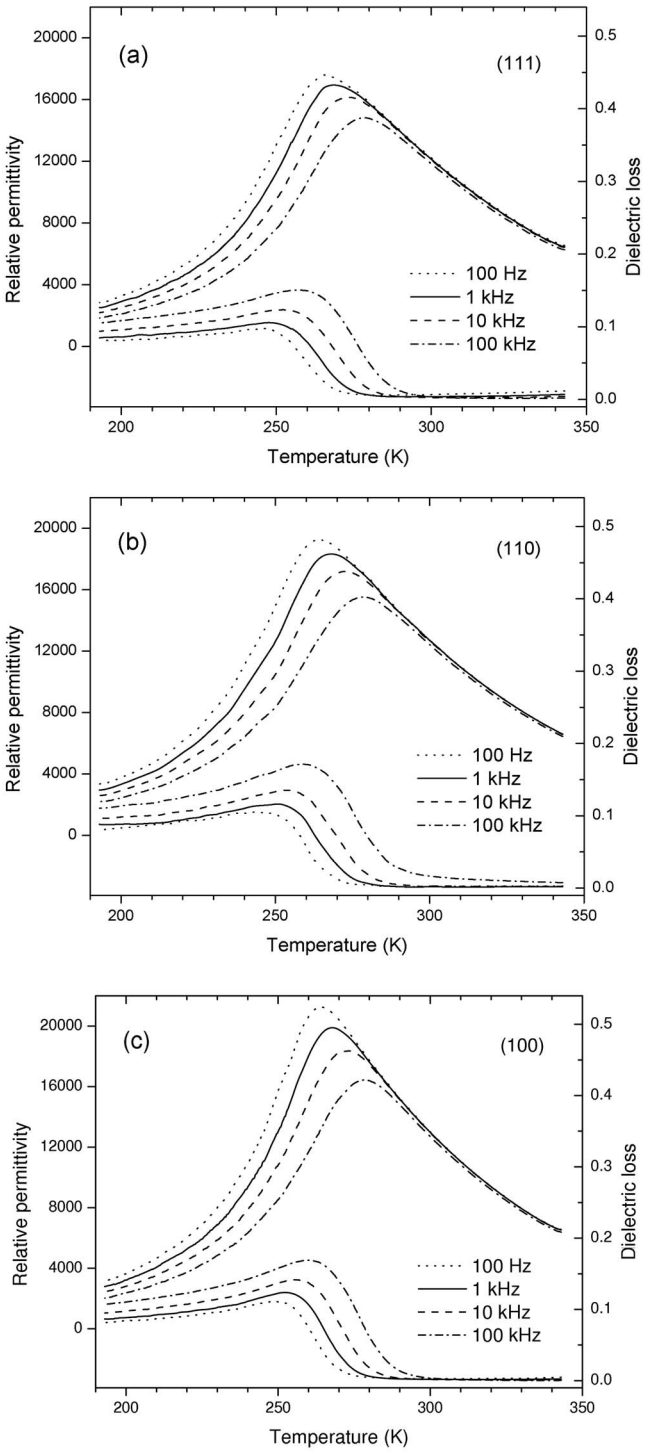

FIG. 1. Dielectric properties of $Pb(Mg_{1/3}Nb_{2/3})O_3$ single crystals measured during cooling under zero bias field. (a) (111), (b) (110), and (c) (100) platelets.

When the field was applied along the ⟨110⟩ direction, much weaker dielectric anomalies were detected at 197 K under 3.0 kV/cm and 222 K under 5.0 kV/cm. At the field level of 7.5 kV/cm, a dielectric anomaly can be barely detected at 232 K [Fig. 3(b)]. For the (100) crystal platelet, no apparent anomaly was observed on the relative permittivity ε_r vs T curves under 3.0, 5.0, or 7.5 kV/cm. However,

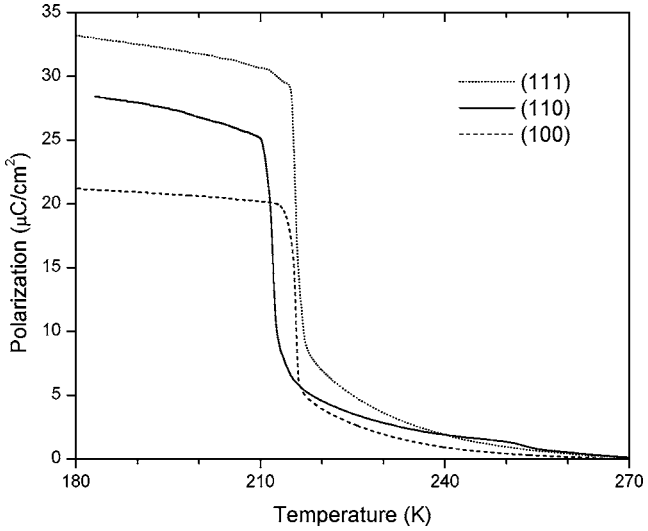

FIG. 2. Development of macroscopic polarization as a function of temperature. The curve is integrated from the thermal depolarization current during zero-field heating after 10 kV/cm field cooling.

anomalies did appear on the tan δ vs T curves at 204 K under 5.0 kV/cm, and 215 K under 7.5 kV/cm [Fig. 3(c)].

D. Dielectric properties upon field heating after field cooling

After the field-cooling tests, field-heating tests were conducted under the same field level. Dielectric permittivity and loss as a function of temperature were measured and are shown in Fig. 4. For the (111) crystal, an anomaly associated with the ferroelectric to relaxor transition upon heating occurs at 230 K under 3.0 kV/cm and 242 K under 5.0 kV/cm, and immerses into the dielectric peak under 7.5 kV/cm [Fig. 4(a)]. For the (110) platelet, the transition occurs at 222 K under 3.0 kV/cm, 230 K under 5.0 kV/cm, and 238 K under 7.5 kV/cm [Fig. 4(b)]. For the (100) platelet, the phase transition can barely be detected from the dielectric loss curve at 218 K under 3.0 kV/cm, but is clearly observed at 226 K under 5.0 kV/cm and at 229 K under 7.5 kV/cm [Fig. 4(c)].

E. Polarization hysteresis measurements

The reversibility of polarization in the field-induced ferroelectric phase was evaluated by polarization vs field ($P \sim E$) hysteresis loop measurement at temperatures below T_m with a peak-to-peak field of ±20 kV/cm. As shown in Fig. 5, all three platelets show well-defined ferroelectric hysteresis loops, indicating reversible macroscopic polarizations within the test temperature range. However, a close examination shows significant differences between the three orientations. For the (111) platelet, the reversible polarization was significantly suppressed at 153 K, compared to that at 173 K (the remanent polarization P_r is 6.0 $\mu C/cm^2$ at 153 K and 25.5 $\mu C/cm^2$ at 173 K). Obviously, a large fraction of the polarization was frozen at 153 K in the (111) platelet, giving rise to a much higher coercive field and a much lower rem-

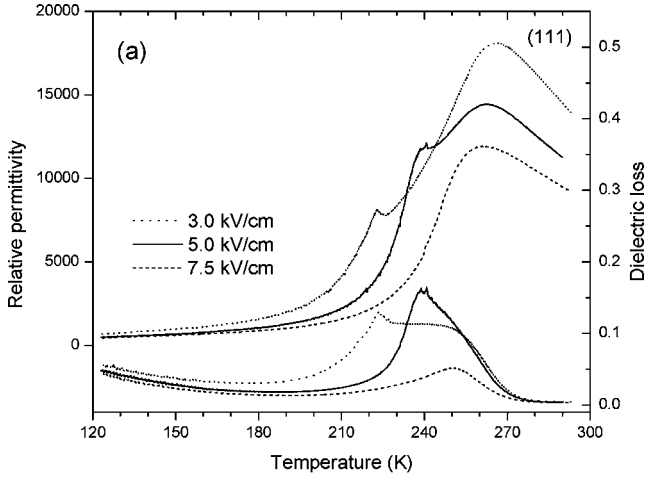

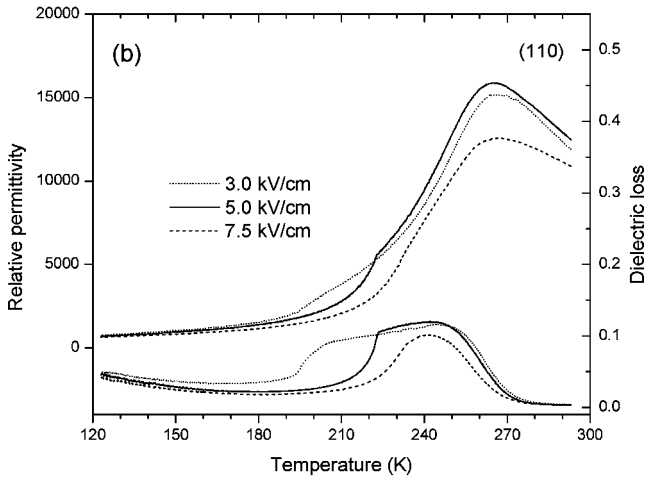

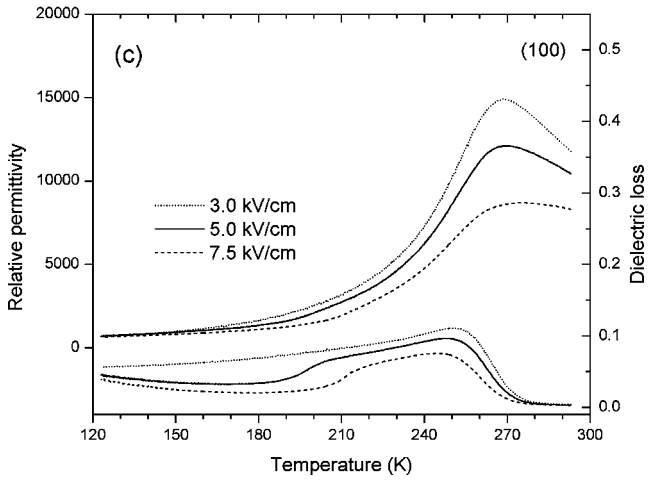

FIG. 3. Dielectric properties of $Pb(Mg_{1/3}Nb_{2/3})O_3$ single crystals measured during field cooling at 1 kHz. (a) (111), (b) (110), and (c) (100) platelets.

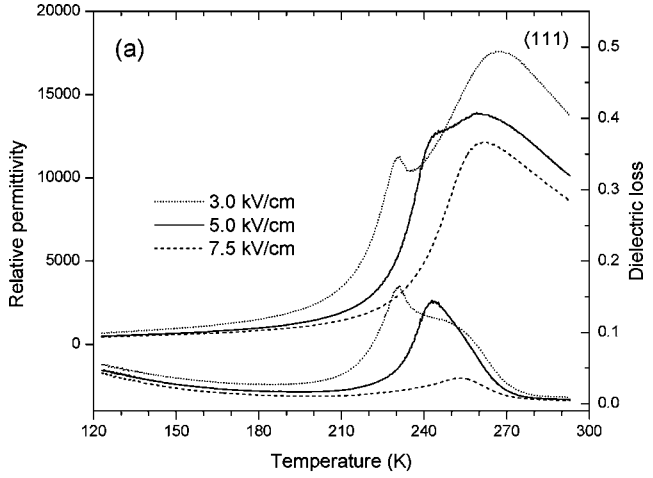

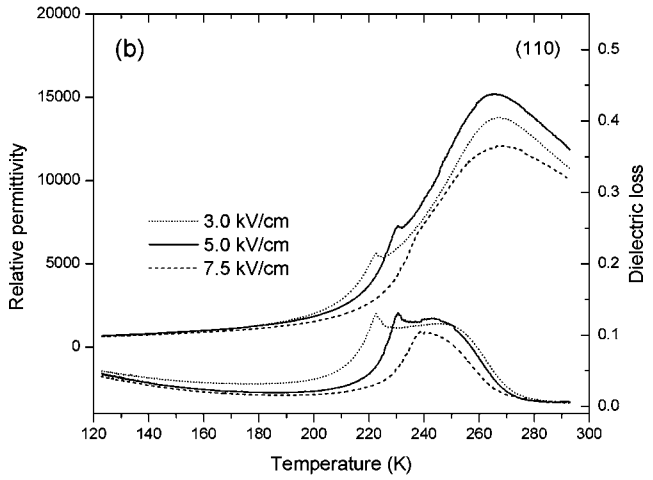

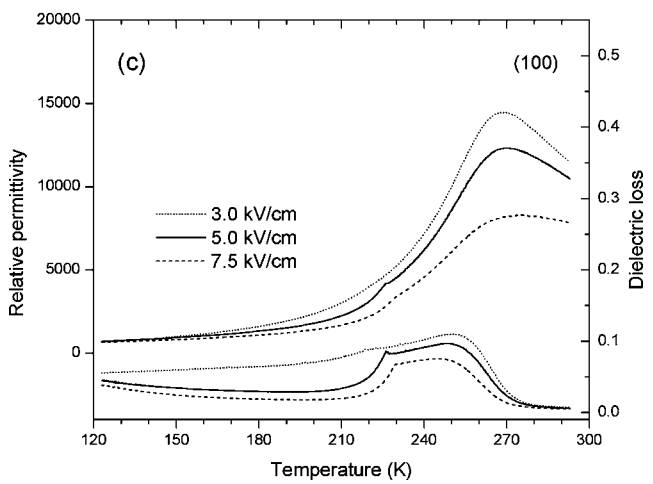

FIG. 4. Dielectric properties of $Pb(Mg_{1/3}Nb_{2/3})O_3$ single crystals measured during field heating after field cooling at 1 kHz. (a) (111), (b) (110), and (c) (100) platelets.

anent polarization. Increasing the temperature from 173 K to 193 K and to 213 K did not significantly change P_r [Fig. 5(a)].

The *P-E* hysteresis loops at different temperatures in the (110) thin crystal show distinct features [Fig. 5(b)]. At 153 K, large reversible polarization can still be seen but it requires a high coercive field E_c. The hysteresis loop is not saturated at the 20 kV/cm field level. Increasing the temperature to 173 K increases the switchable polarization and reduces the coercive field. Further increasing the temperature to 193 K, however, leads to a significant decrease in the P_r, from 26.2 to 12.3 $\mu C/cm^2$. The low P_r persists up to 213 K. For the (100) platelet, fully developed *P-E* hysteresis loops were observed at all four test temperatures [Fig. 5(c)]. The

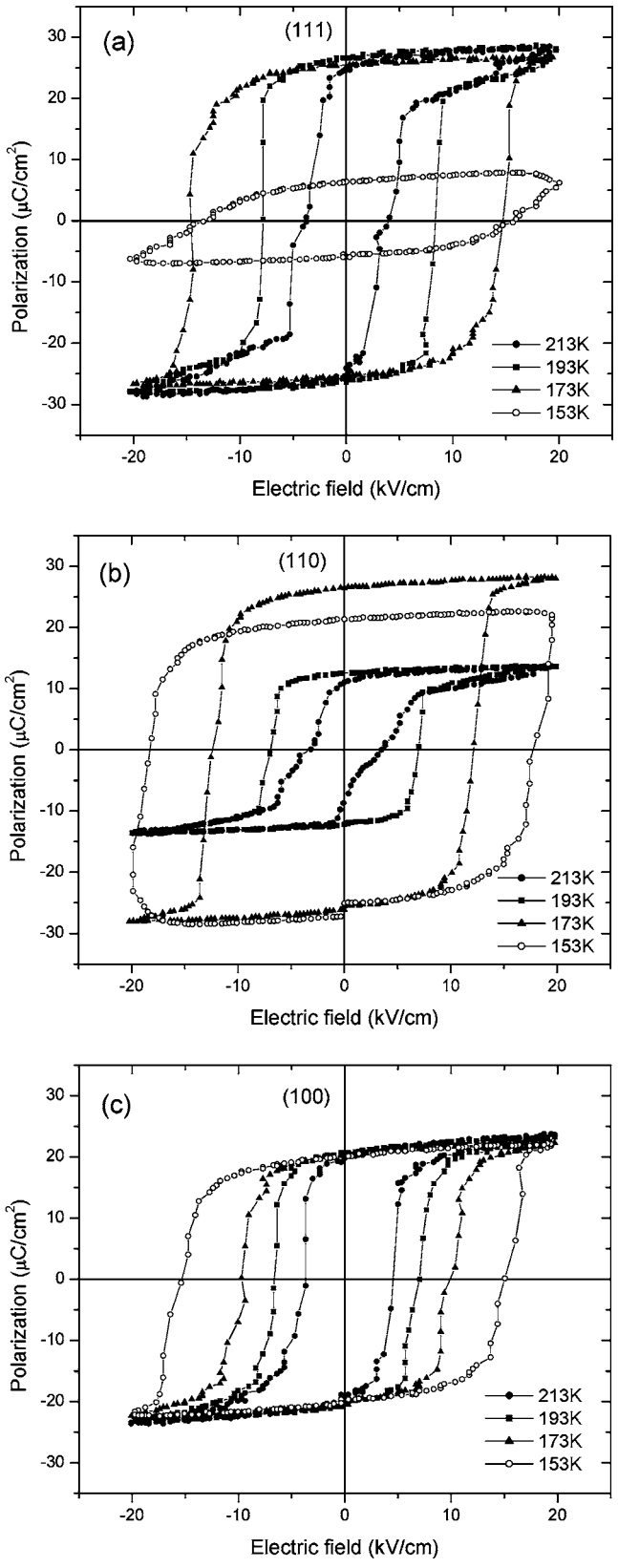

FIG. 5. Polarization vs electric field hysteresis loops measured at 4 Hz under a ±20 kV/cm peak-to-peak field in $Pb(Mg_{1/3}Nb_{2/3})O_3$ single crystals. (a) (111), (b) (110), and (c) (100) platelets.

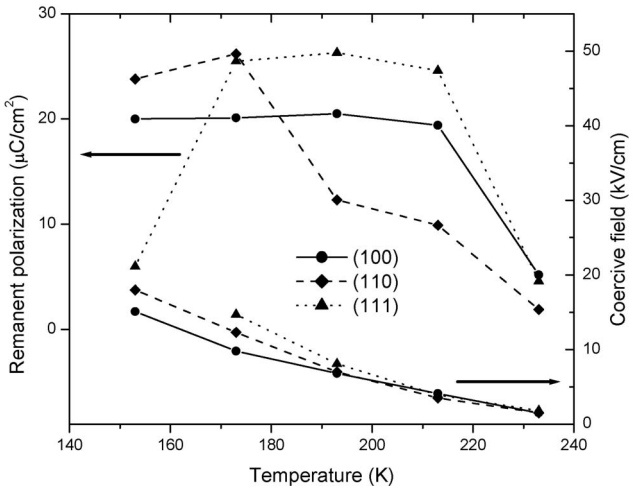

FIG. 6. Remanent polarization P_r and coercive field E_c as a function of temperature in the $Pb(Mg_{1/3}Nb_{2/3})O_3$ single crystals. The $E_c(T)$ lines will be replotted in Fig. 9 to delimit the ferroelectric phase from the glassy nonergodic relaxor phase.

coercive field E_c decreases dramatically, but the remanent polarization P_r remains almost constant as temperature increases from 153 K to 213 K.

The remanent polarization P_r and coercive field E_c measured from the P-E hysteresis loops in Fig. 5, as well as from the hysteresis loops measured at 233 K under 20 kV/cm (not shown) are plotted against temperature in Fig. 6. It is evident that E_c decreases as temperature increases for all three orientations. However, there exists a strong orientation dependence of the remanent polarization P_r. At the highest test temperature (233 K), slim loops with low P_r were recorded for all three crystal slices.

IV. DISCUSSION

The experimental data shown in Figs. 2–6 revealed the electric field-induced phase transition in PMN single crystals. As noted in the Introduction section, phase transition in PMN has been largely studied in (111) thin crystals with the field applied along the ⟨111⟩ direction. Different phases stabilized with combined electric field and temperature conditions are presented in E-T phase diagrams for such experimental configuration.[19–21,23–25] However, such phase diagrams for the (110)- and (100)-oriented PMN single crystals have not yet been reported. Strong orientation dependence of the electric field-induced phase transition has been observed in normal ferroelectrics with the perovskite structure, such as $BaTiO_3$,[35,36] as well as in relaxor-based solid solutions $Pb[(Mg_{1/3}Nb_{2/3})_{1-x}Ti_x]O_3$.[28,37,38] The orientation dependence in these ferroelectric oxides has been clearly illustrated by their distinct E-T phase diagrams.[36,38] As seen in Sec. III, significantly different dielectric and ferroelectric behavior has also been observed in pure PMN crystals with different orientations. Therefore, E-T phase diagrams for the (110)- and (100)-oriented crystals are distinctly different from those for the (111)-oriented crystals.

The relaxors at low temperatures are known to be nonergodic,[39] so that many different thermodynamically

metastable states (or even different phases) may correspond to the same set of thermodynamic parameters (T and E in our case). The phase diagram obtained from experiment is expected to be affected by thermal and field history and different diagrams can be constructed, depending on the paths by which the points of the diagram are reached. It is sensible to choose the state at $T \gg T_m$ as "reference point:" this state is ergodic, and thus truly in equilibrium regardless the history. For that reason we always started the new experiment after annealing the crystal at 373 K $\gg T_m$.

A. Constant-field *E-T* phase diagrams

Figure 7(a) presents the *E-T* phase diagram for the ⟨111⟩ direction based on the results of field cooling and field heating after field-cooling runs at constant fields. Alongside with the T_C values found in the dielectric measurements of the present work (Figs. 3 and 4), the data for T_C extracted from the pyroelectric measurements in Refs. 26 and 31 are also shown. The lowest threshold field level E_{th} that triggers a ferroelectric state in a (111) thin crystal was measured to be 1.75 kV/cm before,[20] thus the low-field boundary of the ferroelectric phase is shown by the horizontal line at this field. The intrinsic Curie temperature T_{C0} (i.e., zero-field-heating after field-cooling value of T_C) determined in Sec. IIB is shown by the arrow. As reported previously,[21,40] it coincides with the glassy freezing temperature T_f separating the ergodic and the glassy nonergodic relaxor phases in the zero-field-cooling regime. The boundary between these two phases at nonzero fields is not known and we can only tentatively mark it by the vertical dashed line. Note that one more phase boundary between the "paraelectric" and "glass-like" states (a nearly vertical line at ~240 K) was reported previously based on the measurements of nonlinear dielectric permittivity.[23,24] However, we have not found in this work any experimental data that would confirm the existence of such a boundary. Thus, it is not shown in Fig. 7(a).

One can see in Fig. 7(a) that the transition temperature between the ferroelectric and ergodic relaxor phases, T_C, is significantly lower on cooling than on subsequent heating (shown by the thick horizontal arrows). Such kind of hysteresis indicates a first-order phase transition. For the position of T_m [which is also shown in Fig. 7(a)] the hysteresis is practically absent. The hysteresis of T_C dramatically decreases with increasing field. At the highest applied field the dielectric anomaly corresponding to T_C can hardly be seen; even if it exists it is smoothed out and immersed into the dielectric peak at T_m [Fig. 3(a) and Fig. 4(a)]. However, at high fields the thermal hysteresis further decreases as can be concluded from the comparison of dielectric curves on heating and cooling at 7.5 kV/cm. According to Ref. 28 decreasing hysteresis and smearing anomaly in response to increasing field in PMN and $Pb(Mg_{1/3}Nb_{2/3})O_3$-$PbTiO_3$ solid solution signify the approaching to a critical endpoint at which the line of the first-order phase transitions in the *E-T* phase diagram terminates. At fields above the critical one the difference between high- and low-temperature phases disappears.

In the (110) and (100) platelets, however, dielectric anomalies are still detected under 7.5 kV/cm [Figs. 3(b), 3(c), 4(b), and 4(c)] and the line of the first-order phase transitions at T_C can be reliably constructed up to this field as shown in Figs. 7(b) and 7(c). It is apparent that the boundary

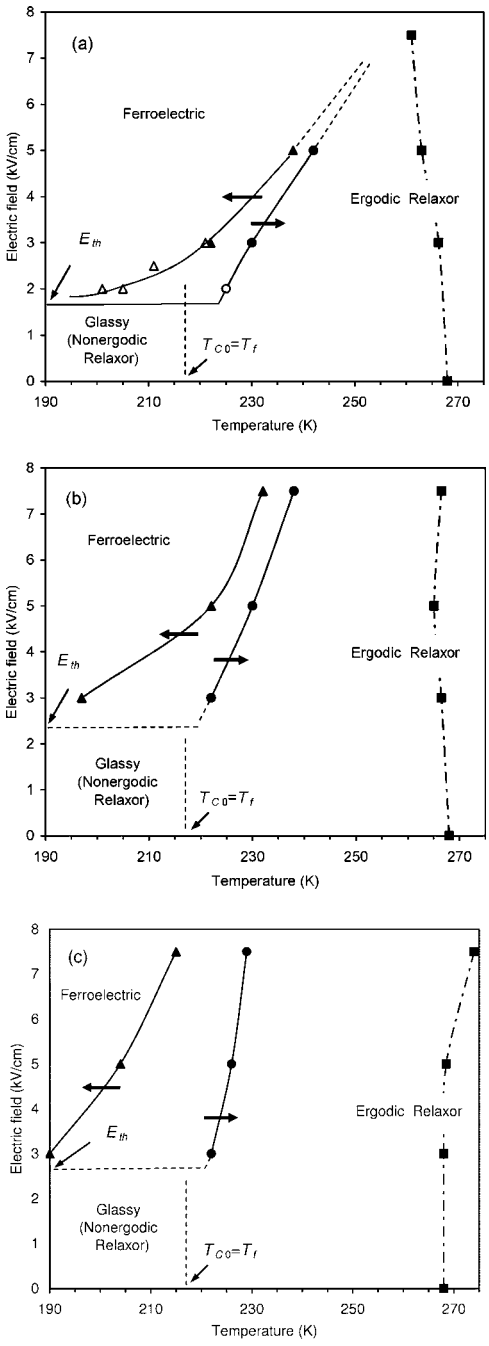

FIG. 7. The *E-T* phase diagrams for $Pb(Mg_{1/3}Nb_{2/3})O_3$ single crystals established based on the processes of field cooling at a constant field and subsequent heating at the same field applied along (a) ⟨111⟩, (b) ⟨110⟩, and (c) ⟨100⟩ directions. The directions of the thermal paths are shown by the thick arrows. The values of T_C upon cooling and heating are shown by triangles and circles, respectively. Solid and dashed lines indicate the boundaries between the ferroelectric, ergodic relaxor and nonergodic relaxor phases. Squares and dotted-dashed line show T_m at 1 kHz. Filled symbols are the results of the present work while open symbols in (a) represent the data from Refs. 26 and 31.

of the ferroelectric region is significantly shifted to lower temperatures under electric fields with directions in the sequence of ⟨111⟩, ⟨110⟩, and ⟨100⟩. Besides, the thermal hysteresis of T_C increases in the same sequence. Cooling and heating T_C lines in the cases of (110) and (110) samples become nearly parallel with increasing field, suggesting that the hysteresis disappears only at very high field (if at all). Therefore, when the field is applied along the ⟨110⟩ or ⟨100⟩ direction, the ferroelectric transition remains far from the critical point even at the highest applied fields and may not reach it at all.

From Figs. 3 and 4, it can be seen that at low fields the dielectric anomalies at T_C are much more smeared for the (110) platelet and especially for the (100) platelet, than for the (111) one. The smearing at low fields suggests the proximity of E_{th}.[20] Again, E_{th} seems to increase in crystals with the field applied in the direction sequence of ⟨111⟩, ⟨110⟩, and ⟨100⟩. The values of E_{th} are tentatively shown in Figs. 7(b) and 7(c) by dashed line.

To explain the peculiarities of the E-T phase diagrams depicted in Fig. 7, we apply the two-stage kinetic model of first-order diffuse phase transitions in compositionally disordered crystals,[41] with the implication that in the PMN relaxor the diffuse ferroelectric transition begins on cooling at Burns temperature. At this temperature the polar nanoregions (PNRs) start to nucleate in the nonpolar matrix, however, the development of the ferroelectric phase is prevented by the compositional disorder, i.e., PMN can be considered as an incipient ferroelectric. This model has been successfully used for the interpretations of the structural changes and T-x phase diagram in the system of $(1-x)Pb(Mg_{1/3}Nb_{2/3})O_3$-$xPbTiO_3$ solid solutions[42] and the dielectric and elastic properties in this system.[43] The model predicts that in the first, high-temperature, stage of the phase transition upon zero field cooling, a PNR is characterized by a specific dependence of its free energy (F) on its size (R). Namely, F first decreases with increasing R and then increases so that the minimum at R_{min} exists which determines the equilibrium size of the PNR. The value of R_{min} can be different for different PNRs and generally increases on cooling. As the equilibrium size of every PNR ($=R_{min}$) is a single-valued function of temperature, the temperature hysteresis is absent at this stage. The PNR can be considered as an individual dipole moment with the magnitude (which is expected to be roughly proportional to R) determined by R_{min} and the direction allowed by the symmetry (eight possible ⟨111⟩ directions in the case of rhombohedral symmetry of PNRs). Therefore the PNR is characterized by an energy structure with eight potential wells separated by barriers. If the temperature is high enough ($T \gg T_f$), the PNRs may be reoriented by thermal fluctuations among the allowed directions (potential wells) and the orientational polarization and relaxation of PNRs in the electric field gives rise to the familiar diffuse and dispersive dielectric maximum at T_m (see Fig. 1). In spite of the fact that the transition is a first-order one, the maximum is nonhysteretic according to the model, which has been confirmed in the experiments.

In the second stage which begins when the crystal is cooled closer to the mean temperature of phase transition, a maximum appears in the $F(R)$ dependences for some (not all) PNRs alongside with the minimum (see Ref. 41 for details). The maximum is located at $R_{max} > R_{min}$ and $F(R)$ becomes a decreasing function for $R > R_{max}$. Such kind of PNRs are therefore metastable. The magnitude of the maximum decreases on further cooling so that at a certain temperature the thermally activated jump over the maximum from the (metastable) state with $R=R_{min}$ to the state with lower energy at $R \gg R_{max}$ becomes possible. This process is analogous to the process of critical nucleation and growth of the new phase in the case of a normal first-order phase transition (see, e.g., Ref. 44) and it is associated with thermal hysteresis. However, in contrast to a normal transition, the activation energy for the formation of the critical nucleus of the ferroelectric phase from the metastable PNR [i.e., the magnitude of $F(R)$ maximum] can be very different for different PNRs, so that the nucleation process is smeared out over a wide temperature range. Besides, the extensive growth of nucleus is impossible because a large number of closely located neighboring PNRs and nuclei hinder the growth. The directions of PNR dipole moments are random. Merging of PNRs into single ferroelectric (macroscopic) domain requires in most cases reorientation of the dipole moments to align them in the same direction. However, the dipole moments are effectively frozen due to the glassy interactions and/or the low temperature (approaching T_f), and their flipping is practically forbidden. As a result, the ferroelectric phase (i.e., the state with macroscopic ferroelectric domains) cannot develop.

When a strong dc field is applied to the crystal at $T \gg T_f$ in the ⟨111⟩ direction, one of the eight potential wells becomes much deeper, and consequently the preferable ⟨111⟩ orientation for PNRs appears. This state can be frozen in the field-cooling process. If the field is high enough, all or almost all PNRs are oriented along the direction of the field (i.e., the subsystem of PNRs is completely poled). Therefore, at the second stage of the transition the growth and mergence of critical nuclei from the metastable PNRs can easily lead to large domains at T_C, giving rise to the formation of the ferroelectric state. Due to the above-mentioned distribution of the temperatures of critical nuclei formation, the transition is diffuse and no sharp anomalies of permittivity and other properties appear. Upon subsequent heating (field heating after field cooling) the crystal transforms back to the ergodic relaxor state with the temperature hysteresis inherent in the first-order transition.

If the dc field is not high enough, PNRs are poled incompletely during field cooling, i.e., some of them retain at $T > T_C$ the directions different from the direction of the field and thereby hinder the growth of ferroelectric phase. As a result, a structure consisting of differently oriented frozen PNRs, supercritical ferroelectric nuclei and nonpolar regions appears. This structure implies the existence of large internal stresses and electric fields which increase on cooling when more and more nuclei form. The stresses and electric fields can be significantly released by the transformation into the state with large ferroelectric domains; however, there exists an energy barrier to the transformation which is related to the (necessary) reorientation of the dipole moments of the struc-

ture inside the frozen "unpoled" PNRs. The reorientation (phase transformation) may happen via the flipping of PNR dipole moments and/or via the motion of the boundaries of ferroelectric phase regions in such a way that their volume fraction increases at the expense of "unpoled" (energetically unfavorable) regions. This appears to be possible if $E > E_{th}$ (the amount of "unpoled" PNRs, and thus the transformation energy barrier, are comparatively small), or impossible if $E < E_{th}$. Nevertheless, the transformation temperature is decreased as compared to the T_C expected in a completely poled crystal at the same field.

Whatever the strength of the field in the field-cooling process, the induced ferroelectric phase is qualitatively the same. Therefore T_C on heating after field cooling is expected to be independent of the field strength on cooling. The increase in the field-heating T_C with E is of the same origin as in the case of any normal ferroelectric transition (see, e.g., Ref. 45). The field-cooling T_C, in contrast, depends also on the PNR reorientation conditions: as discussed above, if E is not high enough, some PNRs need to be reoriented at the transition, which leads to an additional decrease of T_C. This explains the significant enlargement of the temperature hysteresis of T_C with decreasing field (Fig. 7).

If the dc field is applied along ⟨110⟩ or ⟨100⟩, complete poling of PNRs in the course of field cooling at $T > T_C$ is impossible. Indeed, out of the eight ⟨111⟩ directions allowed for the dipole moment of PNRs by the rhombohedral symmetry, two or four directions correspond to the same energy in the case of ⟨110⟩ or ⟨100⟩ field, respectively. Therefore, when the crystal is cooled to T_C, the inevitable PNR reorientations should accompany the process of PNR merging into ferroelectric domains at any field strength. As a result, E_{th} and thermal hysteresis are increased and T_C is decreased [Figs. 7(b) and 7(c)]. In particular even in highest ⟨100⟩ fields, when the maximum possible degree of PNR polarization is achieved at $T > T_C$, additional 71° and 109° reorientations are needed to form the ferroelectric state at T_C. In the ⟨110⟩ field, only 71° reorientations are required, so that the energy barriers are lower than in the ⟨100⟩ case and the effect on T_C, E_{th} and thermal hysteresis is smaller.

B. Constant temperature after zero-field-cooling *E-T* phase diagram

Another type of *E-T* phase diagram can be roughly estimated from the hysteresis loops results (Figs. 5 and 6), namely, the diagram resulting from field application at constant temperature after zero-field cooling. Note that the *E-T* phase diagram constructed after zero-field cooling for the PMN (111) platelet in different modes is known.[20] In that diagram the temperature T_{ph} at which the glassy nonergodic relaxor state transforms to the ferroelectric state was determined after zero-field cooling down to very low temperature during the constant-field-heating tests. The ferroelectric state appears in the diagram within a U-shaped region, bounded by the $T_{ph}(E)$ line at low temperatures and the $T_C(E)$ line at high temperatures.[20,21] The latter line coincides with the $T_C(E)$ line in the field-heating after field-cooling diagram and above T_C the ergodic relaxor state is stable. Based on the results of the present work we try to locate the line separating the cubic glassy phase and the ferroelectric phase in the experiments with isothermal field applied after zero-field cooling. It is expected to coincide with the $T_{ph}(E)$ line, at least approximately.

For the (111) platelet, the reversible polarization determined from the hysteresis loops at 153 K is significantly smaller than that at 173 K. This can be explained in different ways. The first possible explanation is that the crystal remains in the glassy phase (at least partially), i.e., for the field of 20 kV/cm (peak value of E) the temperature of experiment (153 K) is lower than T_{ph}. Alternatively, one may expect that the crystal is in the ferroelectric phase ($T_{ph} < 153$ K at 20 kV/cm) but the peak field is smaller than the coercive field so that the polarization cannot be fully switched. However, it was experimentally confirmed for the ⟨111⟩ direction in PMN, that the $T_{ph}(E)$ line in the phase diagram coincides with the $E_c(T)$ line,[20] i.e., the minimum field needed to induce the ferroelectric phase from the glassy one at some temperature after zero-field cooling equals the coercive field of the ferroelectric phase at this temperature. Therefore, the first explanation is valid, implying that 153 K is lower than the temperature T_{ph} at 20 kV/cm.

The hysteresis loops for the ⟨111⟩ field at higher temperatures [shown in Fig. 5(a)] are saturated, i.e., the peak field applied is higher than E_c and the E_c value can be measured (as the intersection of the loop with the abscissa axis) and subsequently used for determining the line of phase transition from the glassy phase to the ferroelectric phase. As explained above, it is the same as the $E_c(T)$ line.

For the (110) platelet, the reversible polarization is only slightly suppressed at 153 K while for the (100) crystal, the reversible polarization is not at all suppressed at 153 K. Therefore, the $T_{ph}(E)$ line for the (100)-oriented crystal should be located at lower temperatures than that for the (110)-oriented crystals, and both of them are at lower temperatures than the (111)-oriented crystals. In order to more accurately locate the $T_{ph}(E)$ line for the ⟨100⟩ field orientation, the (100) crystal platelet was further tested for reversible polarization at liquid nitrogen temperature (77 K). The results are shown in Fig. 8. It is evident that the polar order is completely frozen and cannot be reversed at ±20 kV/cm. A saturated *P-E* hysteresis loop cannot be achieved even under ±40 kV/cm (only a very small P_r of 1.2 μC/cm^2 is measured from the loop). Therefore, the $T_{ph}(E)$ line for the (100)-oriented PMN crystal should lie above 77 K for electric fields below 40 kV/cm.

The above discussion is summarized in Fig. 9. Alongside with $T_C(E)$, the diagrams establish the $T_{ph}(E)$ lines for different orientations of the field. The diagrams include the following features: (a) the ferroelectric state with reversible polarization is confined within a U-shaped region for all three orientations; (b) below this region the ergodic relaxor phase is observed at temperatures above $\sim T_f$; at lower temperatures the state can be nonergodic relaxor (before the first field application) or ferroelectric with nonreversible polarization (if $E > E_c$ has already been applied); and (c) the U-shaped region shifts to lower temperatures and to higher fields in crystals with orientations in the sequence of (111), (110), and (100).

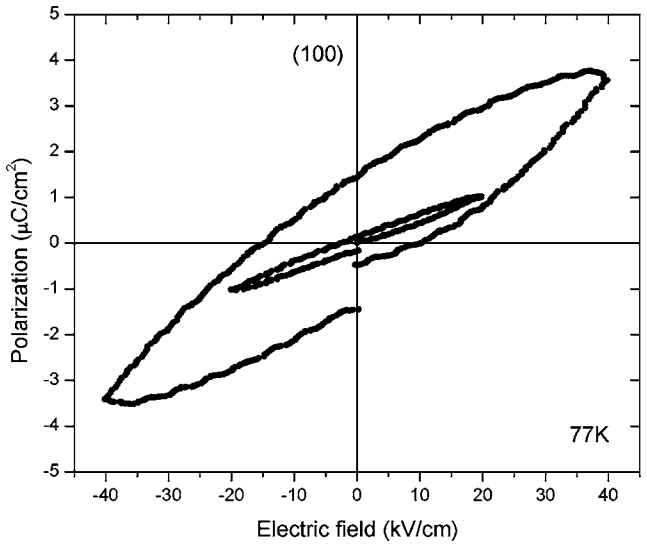

FIG. 8. Polarization vs electric field hysteresis loops measured at 4 Hz under ±20 kV/cm and ±40 kV/cm peak-to-peak fields in the (100)-oriented $Pb(Mg_{1/3}Nb_{2/3})O_3$ crystal at 77 K.

One can notice that the easiest way to induce the ferroelectric phase from the high-temperature ergodic relaxor phase is to apply the field in the ⟨111⟩ direction. In particular, E_{th} for this direction is smaller and T_C (at the same E) is higher than for other directions. On the contrary, for the ferroelectric transition from the glassy phase at $T \ll T_f$ the ⟨111⟩ direction is the "hardest" one. This behavior can be understood from the fact that the PNRs are completely frozen at $T \ll T_f$ and the mechanisms of transformation discussed in Sec. IV A implying the flipping of PNR dipole moments no longer work. It seems that the process of field-induced merging of nanoscale polar regions of glassy phase into large domains of ferroelectric phase is similar to the poling process in normal ferroelectrics. In the latter case the dipole moments of domains are also frozen and it is the motions of domain walls that allow the crystal to be poled effectively rather than the switching of the whole domains.[45] Likewise, the polar regions of glassy relaxor phase whose dipole moment directions are parallel (or close) to the direction of the poling field grow and absorb the other polar regions. This mechanism is in agreement with the above-mentioned finding that at $T \ll T_f$ the same lowest field is needed to reverse the polarization in the ferroelectric phase (i.e., E_c) and to induce the ferroelectric phase from the glassy one.

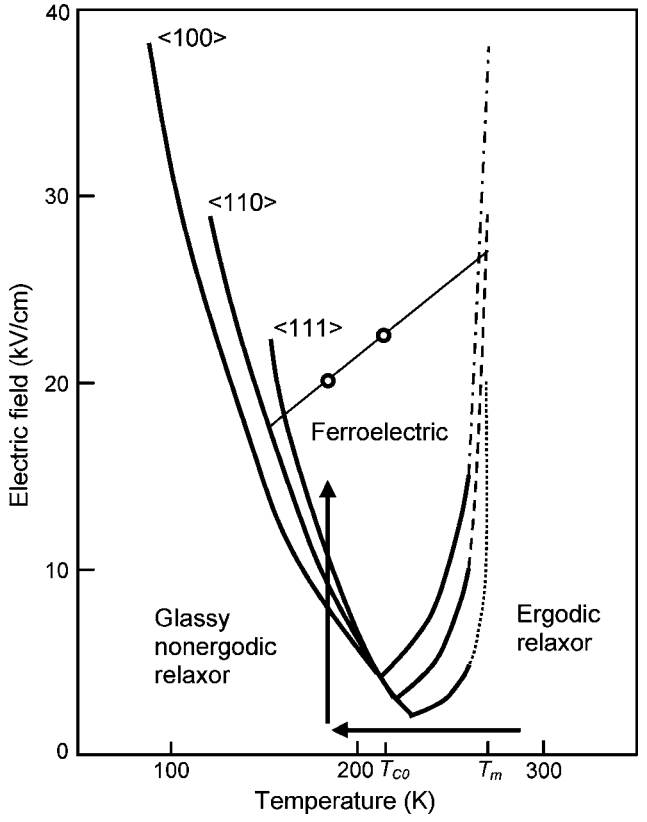

FIG. 9. The E-T phase diagrams of $Pb(Mg_{1/3}Nb_{2/3})O_3$ single crystals obtained from data presented in Figs. 6 and 7. The $E_c(T)$ or $T_{ph}(E)$ lines, delimiting the ferroelectric phase from the glassy nonergodic phase were attained from the measurement of ferroelectric hysteresis loops in different directions after zero-field cooling. The directions of the employed E-T path are shown by thick arrows.

C. Further ferroelectric-to-ferroelectric phase transitions

The electric field-induced phase transition in PMN is presumably different from that in normal ferroelectrics such as $BaTiO_3$ because of the distinct nature of their polar structures. The polar nanoregions in PMN are known to have local rhombohedral symmetry with polarization fluctuating along all the eight ⟨111⟩ directions.[2,9–15] It is highly probable that if the field is not very high the electric field-induced phase transition in PMN is a cubic-to-rhombohedral structural transition, regardless of the direction of the applied electric fields. In fact, such field-induced macroscopic rhombohedral structure was speculated by Schmidt *et al.*[29] in 1980 in their pioneering studies on (111), (110), and (100) PMN crystals. It was later found that when the field was applied along the ⟨111⟩ direction, a monodomain state could be easily achieved, while the fields applied in the ⟨110⟩ and ⟨100⟩ directions always result in a multidomain state.[20,31] As mentioned in Sec. III B, the values of the induced polarization under 10 kV/cm field cooling support the idea of the cubic-to-rhombohedral phase change.

Further ferroelectric-to-ferroelectric phase transition may occur in PMN single crystals under strong electric fields. It has been theoretically shown that in normal ferroelectrics with the perovskite structure, the rhombohedral, orthorhombic, and tetragonal phases have close free energies and, depending on the field direction, external electric fields can stabilize any one of them.[36,46,47] The transition is realized through a polarization rotation process, which often leads to intermediate monoclinic phases.[46,47] We believe that it is also possible for further ferroelectric-to-ferroelectric transitions to occur in PMN at high electric fields. For the (111)-oriented crystal with field applied along the ⟨111⟩ direction, the rhombohedral structure will be stable and since the field direction is parallel to the polarization direction, there will be no further ferroelectric-to-ferroelectric transition. For the (110)

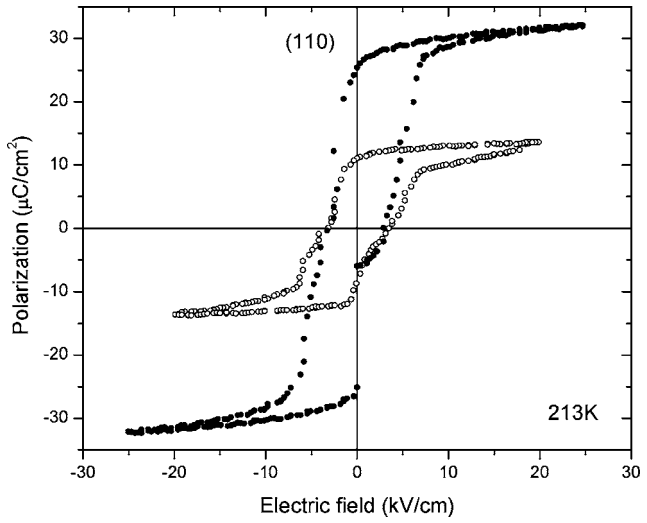

FIG. 10. Polarization vs electric field hysteresis loops measured at 4 Hz under ±20 kV/cm and ±25 kV/cm peak-to-peak fields in the (110)-oriented $Pb(Mg_{1/3}Nb_{2/3})O_3$ crystal at 213 K.

platelet with field applied along the ⟨110⟩ direction, a further ferroelectric rhombohedral to ferroelectric orthorhombic phase transition may be triggered. While for the (100) platelet, a further ferroelectric rhombohedral to ferroelectric tetragonal transition may be triggered under high electric fields. These transitions were previously suggested to account for the ultrahigh piezoelectric strains in rhombohedral $Pb[(Mg_{1/3}Nb_{2/3})_{1-x}Ti_x]O_3$ single crystals.[28,48,49]

The abnormal change in the remanent polarization P_r in the (110)-oriented crystal shown in Fig. 5(b) and Fig. 6 suggests that the ferroelectric rhombohedral to ferroelectric orthorhombic transition actually may have occurred in the (110) platelet. The hysteresis loops presented in Fig. 5(b) appear to indicate that the 20 kV/cm electric field stabilizes an orthorhombic phase at 153 K and 173 K, but a rhombohedral phase at 193 K and 213 K. Therefore, there is an additional line delimiting the ferroelectric rhombohedral and the ferroelectric orthorhombic phases within the U-shaped region in the *E-T* phase diagram for the (110)-oriented crystal (Fig. 9). This line passes the point (183 K, 20 kV/cm), where 183 K is the midpoint between 173 K and 193 K. The orthorhombic phase is favored at high electric fields while the rhombohedral phase is favored at low electric fields.

In order to locate a second point on the rhombohedral-orthorhombic phase boundary line, the remanent polarization P_r in the (110) crystal platelet was further measured at 213 K under electric fields of ±25, ±30, ±35, and ±40 kV/cm along the ⟨110⟩ direction. The *P-E* hysteresis loops are shown in Fig. 10. Consistent with the proposed rhombohedral-to-orthorhombic phase transition, P_r abruptly increases from 9.9 $\mu C/cm^2$ under ±20 kV/cm to 25.2 $\mu C/cm^2$ under ±25 kV/cm at this temperature. The P_r value remains around 25 $\mu C/cm^2$ under±30, ±35, and ±40 kV/cm. Therefore, the rhombohedral-orthorhombic phase boundary line in the *E-T* phase diagram for the (110) crystal platelet passes a second point (213 K, 22.5 kV/cm). These two experimentally determined data points are marked in Fig. 9 as open circles.

In the following, we analyze the values of the remanent polarization to further support the proposed ferroelectric rhombohedral to ferroelectric orthorhombic phase transition in the (110)-oriented crystal. At 173 K, a ferroelectric orthorhombic phase is resulted from the ferroelectric rhombohedral phase under 20 kV/cm. This transition presumably leads to a polarization vector parallel to the direction of the applied field, the $\langle 110\rangle_{cubic}$ direction. Therefore, a high P_r is expected. From Fig. 6, it can be seen that the P_r for the induced orthorhombic phase (26.2 $\mu C/cm^2$ at 173 K) is indeed high and is comparable to that of the monodomain rhombohedral phase (25.5 $\mu C/cm^2$ at 173 K).

However, in the present study, the ferroelectric rhombohedral to the ferroelectric tetragonal phase transition was not observed with field up to 40 kV/cm in the (100) platelet crystal, indicating that such transition may require a much higher field.

V. CONCLUSIONS

The electric field-induced phase transition was investigated in $Pb(Mg_{1/3}Nb_{2/3})O_3$ single crystals with the field applied along the ⟨111⟩, ⟨110⟩, and ⟨100⟩ directions and *E-T* phase diagrams have been constructed. Because of nonergodicity effects the low-temperature part of the diagram depends dramatically on the history of the crystal. The diagrams based on the results of field-cooling and field-heating after field-cooling experiments are shown in Fig. 7. The diagrams in Fig. 9 depict for all three directions the U-shaped region of the ferroelectric state which was found in experiments with isothermal field application after zero-field cooling. The Curie temperature T_C (the upper boundary of the U-shaped region) and the lower boundary of the U-shaped region are shifted to lower temperatures in the crystal under field directions in the sequence of ⟨111⟩, ⟨110⟩, and ⟨100⟩. The electric field along the ⟨111⟩ and ⟨100⟩ directions trigger only the relaxor cubic to ferroelectric rhombohedral phase transition. Fields along the ⟨110⟩ direction with a magnitude around 20 kV/cm trigger a further ferroelectric rhombohedral to ferroelectric orthorhombic transition after the initial relaxor cubic to ferroelectric rhombohedral transition.

The lowest threshold field E_{th} needed to induce ferroelectric phase was measured in the field-cooling experiments. It is found to be the largest in the (100)-oriented crystal with field applied along the ⟨100⟩ direction, and the smallest for the (111)-oriented crystal with field along the ⟨111⟩ direction. In the field cooling and field heating after field-cooling experiments for the ⟨100⟩ and ⟨110⟩ field directions, significant dielectric anomalies and large hysteresis of T_C are revealed which do not vanish even at the highest applied field of 7.5 kV/cm, in contrast to the ⟨111⟩ field direction where the disappearance of anomalies and hysteresis is known to be the result of the critical endpoint existing on the $T_C(E)$ line of the first-order phase transitions. As one can judge from the character of $T_C(E)$ dependences, the critical point for non-⟨111⟩ directions is probably also absent at fields higher than 7.5 kV/cm.

It is suggested that the mechanisms of the field-induced transformation to the ferroelectric phase from the glassy nonergodic relaxor phase and from the ergodic relaxor phase are

different. In the former case the motions of the boundaries between polar nanoregions are the main origin. In the latter case the flipping of the dipole moments of the polar nanoregions are involved. The behavior is explained in terms of the two-stage kinetic model of the first-order phase transitions in compositionally disordered crystals.[41,42]

Note that far reaching implications are attached to our conclusion about the critical point in the *E-T* phase diagram. It was recently suggested that the origin of the giant electromechanical response in ferroelectric relaxors was related to the existence of the critical point at which enhanced piezoelectric coefficients were expected[28,50] and practically observed.[28] All the experiments related to the critical point were conducted in Ref. 28 for the ⟨111⟩ direction of the field only. On the other hand, the electromechanical response in this direction is comparatively moderate; only when the field is applied along ⟨100⟩ it becomes extraordinary large.[48] However, in the present work we do not find the critical point in the ⟨100⟩ direction. Therefore, the relation between the giant electromechanical response and the critical behavior becomes questionable and more experimental efforts are needed to elucidate this intriguing issue.

ACKNOWLEDGMENTS

This work was supported by the National Science Foundation through the CAREER Grant No. DMR-0346819, and by the Office of Naval Research (Grant No. 00014-06-10016).

*Electronic address: xtan@iastate.edu

[1] G. A. Smolensky, J. Phys. Soc. Jpn. **28**, 26 (1970).
[2] L. E. Cross, Ferroelectrics **76**, 241 (1987).
[3] H. B. Krause, J. M. Cowley, and J. Wheatley, Acta Crystallogr., Sect. A: Cryst. Phys., Diffr., Theor. Gen. Crystallogr. **A35**, 1015 (1979).
[4] J. Chen, H. M. Chan, and M. P. Harmer, J. Am. Ceram. Soc. **72**, 593 (1989).
[5] A. D. Hilton, D. J. Barber, C. A. Randall, and T. R. Shrout, J. Mater. Sci. **25**, 3461 (1990).
[6] M. A. Akbas and P. K. Davies, J. Am. Ceram. Soc. **83**, 119 (2000).
[7] Z. Xu, S. M. Gupta, D. Viehland, Y. Yan, and S. J. Pennycook, J. Am. Ceram. Soc. **83**, 181 (2000).
[8] G. Burns and F. H. Dacol, Solid State Commun. **48**, 853 (1983).
[9] P. Bonneau, P. Garnier, G. Calvarin, E. Husson, J. R. Gavarri, A. W. Hewat, and A. Morell, J. Solid State Chem. **91**, 350 (1991).
[10] A. Naberezhnov, S. Vakhrushev, B. Dorner, D. Strauch, and H. Moudden, Eur. Phys. J. B **11**, 13 (1999).
[11] H. Hiraka, S.-H. Lee, P. M. Gehring, G. Xu, and G. Shirane, Phys. Rev. B **70**, 184105 (2004).
[12] N. Takesue, Y. Fujii, and H. You, Phys. Rev. B **64**, 184112 (2001).
[13] R. Blinc, V. Laguta, and B. Zalar, Phys. Rev. Lett. **91**, 247601 (2003).
[14] G. Xu, G. Shirane, J. R. D. Copley, and P. M. Gehring, Phys. Rev. B **69**, 064112 (2004).
[15] I. K. Jeong, T. W. Darling, J. K. Lee, Th. Proffen, R. H. Heffner, J. S. Park, K. S. Hong, W. Dmowski, and T. Egami, Phys. Rev. Lett. **94**, 147602 (2005).
[16] B. P. Burton, E. Cockayne, and U. V. Waghmare, Phys. Rev. B **72**, 064113 (2005).
[17] B. P. Burton, E. Cockayne, S. Tinte, and U. V. Waghmare, Phase Transitions **79**, 91 (2006).
[18] V. Westphal, W. Kleemann, and M. D. Glinchuk, Phys. Rev. Lett. **68**, 847 (1992).
[19] R. Sommer, N. K. Yushin, and J. J. van der Klink, Phys. Rev. B **48**, 13230 (1993).
[20] Z.-G. Ye and H. Schmid, Ferroelectrics **145**, 83 (1993).
[21] Z.-G. Ye, Key Eng. Mater. **155-156**, 81 (1998).
[22] G. Calvarin, E. Husson, and Z. G. Ye, Ferroelectrics **165**, 349 (1995).
[23] E. V. Colla, E. Y. Koroleva, A. A. Nabereznov, and N. M. Okuneva, Ferroelectrics **151**, 337 (1994).
[24] E. V. Colla, E. Y. Koroleva, N. M. Okuneva, and S. B. Vakhrushev, Phys. Rev. Lett. **74**, 1681 (1995).
[25] E. V. Colla and M. B. Weissman, Phys. Rev. B **72**, 104106 (2005).
[26] B. Dkhil and J. M. Kiat, J. Appl. Phys. **90**, 4676 (2001).
[27] R. Blinc, V. V. Laguta, B. Zalar, and J. Banys, J. Mater. Sci. **41**, 27 (2006).
[28] Z. Kutnjak, J. Petzelt, and R. Blinc, Nature (London) **441**, 956 (2006).
[29] G. Schmidt, H. Arndt, J. von Cieminski, T. Petzsche, H. J. Voigt, and N. N. Krainik, Krist. Tech. **15**, 1415 (1980).
[30] H. Arndt, F. Sauerbier, G. Schmidt, and L. A. Shebanov, Ferroelectrics **79**, 145 (1988).
[31] Z.-G. Ye, Ferroelectrics **172**, 19 (1995).
[32] S. G. Lushnikov, A. I. Fedoseev, J. H. Ko, and S. Kojima, Jpn. J. Appl. Phys., Part 1 **44**, 7156 (2005).
[33] Z.-G. Ye, P. Tissot, and H. Schmid, Mater. Res. Bull. **25**, 739 (1990).
[34] C. S. Park, K. Y. Lim, D. Y. Choi, and S. J. Chung, J. Korean Phys. Soc. **32**, S974 (1998).
[35] S. Wada, S. Suzuki, T. Noma, T. Suzuki, M. Osada, M. Kakihana, S. E. Park, L. E. Cross, and T. R. Shrout, Jpn. J. Appl. Phys., Part 1 **38**, 5505 (1999).
[36] A. J. Bell, J. Appl. Phys. **89**, 3907 (2001).
[37] X. Zhao, J. Wang, H. L. W. Chan, C. L. Choy, and H. Luo, J. Phys.: Condens. Matter **15**, 6899 (2003).
[38] H. Cao, J. Li, D. Viehland, and G. Xu, Phys. Rev. B **73**, 184110 (2006).
[39] A. A. Bokov and Z.-G. Ye, J. Mater. Sci. **41**, 31 (2006).
[40] A. A. Bokov and Z.-G. Ye, Phys. Rev. B **74**, 132102 (2006).
[41] A. A. Bokov, Phys. Solid State **36**, 19 (1994).
[42] Z.-G. Ye, Y. Bing, J. Gao, A. A. Bokov, P. Stephens, B. Noheda, and G. Shirane, Phys. Rev. B **67**, 104104 (2003).
[43] R. Jiménez, B. Jiménez, J. Carreaud, J. M. Kiat, B. Dkhil, J. Holc, M. Kosec, and M. Algueró, Phys. Rev. B **74**, 184106 (2006).
[44] J. W. Christian, *The Theory of Transformations in Metals and*

Alloys (Pergamon, Oxford, 1965).
[45] M. E. Lines and A. M. Glass, *Principles and Applications of Ferroelectric and Related Materials* (Clarendon, Oxford, 1977).
[46] H. Fu and R. E. Cohen, Nature (London) **403**, 281 (2000).
[47] D. Vanderbilt and M. H. Cohen, Phys. Rev. B **63**, 094108 (2001).
[48] S. E. Park and T. R. Shrout, J. Appl. Phys. **82**, 1804 (1997).
[49] D. Viehland and J. F. Li, J. Appl. Phys. **92**, 7690 (2002).
[50] R. E. Cohen, Nature (London) **441**, 941 (2006).